Rapid Identification of Lipsticks Using Laser Induced Breakdown Spectroscopy

Zahid Hussain Arain[a], Nek Muhammad Shaikh[a*], Yasir Jamil[b], Saifullah Jamali[a,c], Muhammad Aslam Khoso[a], Meer Hassan Brohi[a]**

[a] Institute of Physics, University of Sindh, Jamshoro 71000, Pakistan
[b] Department of Physics, University of Agriculture, Faisalabad 03802, Pakistan
[c] Anhui Provincial Key Laboratory of Photonic Devices and Materials, Anhui Institute of Optics and Fine Mechanics, Hefei Institutes of Physical Sciences, Chinese Academy of Sciences, Hefei 230031, China

Abstract- Heavy metal contamination in cosmetics is a significant concern due to the potential for chronic health issues from prolonged exposure. This study examines the health risks posed by elemental analysis of lipsticks using Laser-Induced Breakdown Spectroscopy (LIBS). LIBS, recognized for its rapid and precise analytical capabilities, was utilized to detect and quantify toxic elements in various lipstick samples. The experimental setup involved using a Q-switched Nd: YAG laser to generate plasma from the lipstick samples, with the resulting spectral data analyzed to determine their chemical composition. Iron (Fe), Carbon (C), Cobalt (Co), Chromium (Cr), Lead (Pb), Molybdenum (Mo), Barium (Ba), Zinc (Zn) Magnesium (Mg), Calcium (Ca), Cadmium (Cd), Potassium (K), Aluminum (Al), Sodium (Na), Hydrogen (H) and Lithium (Li) were confirmed. Chemometric tools, principal component analysis (PCA) and linear discriminant analysis (LDA) were used to distinguish the lipstick samples. Additionally, plasma parameters such as electron temperature, electron number density, plasma frequency, and inverse bremsstrahlung coefficient were calculated, showing variations with the axial distance from the plasma plume.

Key words- LIBS; Lipstick, Quantitative Analysis, LDA, PCA, Electron Temperature, Electron Number Density, inverse bremsstrahlung coefficient, Plasma Frequency, CF-LIBS

1. INTRODUCTION

Lipstick is widely used in the global beauty market as a beauty product, beside that it has also adverse effects. One of the main concerns is heavy metal contamination, which can lead to significant health risks despite the small amounts of exposure, as these metals can accumulate in the body over prolonged periods of use [1, 2]. Various techniques used to analysis lipstick including EDX [3], Raman spectroscopy [4], thin layer chromatography (TLC) [5], and X-ray diffraction (XRD) [6] etc. Among the available technique Laser-Induced Breakdown Spectroscopy (LIBS) has made considerable strides in recent years due to its multidirectional advantages including rapid analysis, no or little sample preparation, nondestructive and ability to evaluate wide range of elements etc. [7-10]. In this technique, a high-energy laser beam interacts with the sample material, producing a plasma that contains ions, atoms, and electrons. The spectrometer then resolves the light emitted by the plasma to determine the chemical composition of the sample material [11, 12].

Previous studies have shown that heavy metals such as lead can be absorbed through the skin, posing health risks, especially to children and women [2, 13]. Gondal et al. [14] used LIBS to determine the concentration of toxic elements like Pb, Cr, Cd, and Zn in lipsticks sold in Saudi Arabia and found that the concentrations of some metals were much higher than safe permissible limits. Similarly, Liu et al. [15] measured Pb and other metals in 32 lip products used by young Asian women in Oakland, California, using ICP-OES, finding high concentrations of Ti and Al. Asmaa et al., [16] studied laser produced lipstick plasma to estimate plasma parameter. Abrar et al., [17] reported Cr, Mg, Cd, Pb, Mn, Na, P, S, Si, and Ti in laser produced personal care products. However, there are still a lot of obstacles to overcome, even with the development of analytical methods like LIBS and the knowledge gathered from earlier research on heavy metal pollution in lipsticks.

Using Laser-Induced Breakdown Spectroscopy (LIBS), a thorough investigation of lipstick samples was the goal of this study, with an emphasis on finding any harmful and non-toxic components. Furthermore, in order to differentiate between various lipstick brands according to their elemental compositions, chemometric techniques including Principal Component Analysis (PCA) and Linear Discriminant Analysis (LDA) were used. In addition, the study sought to learn more about the thermodynamic

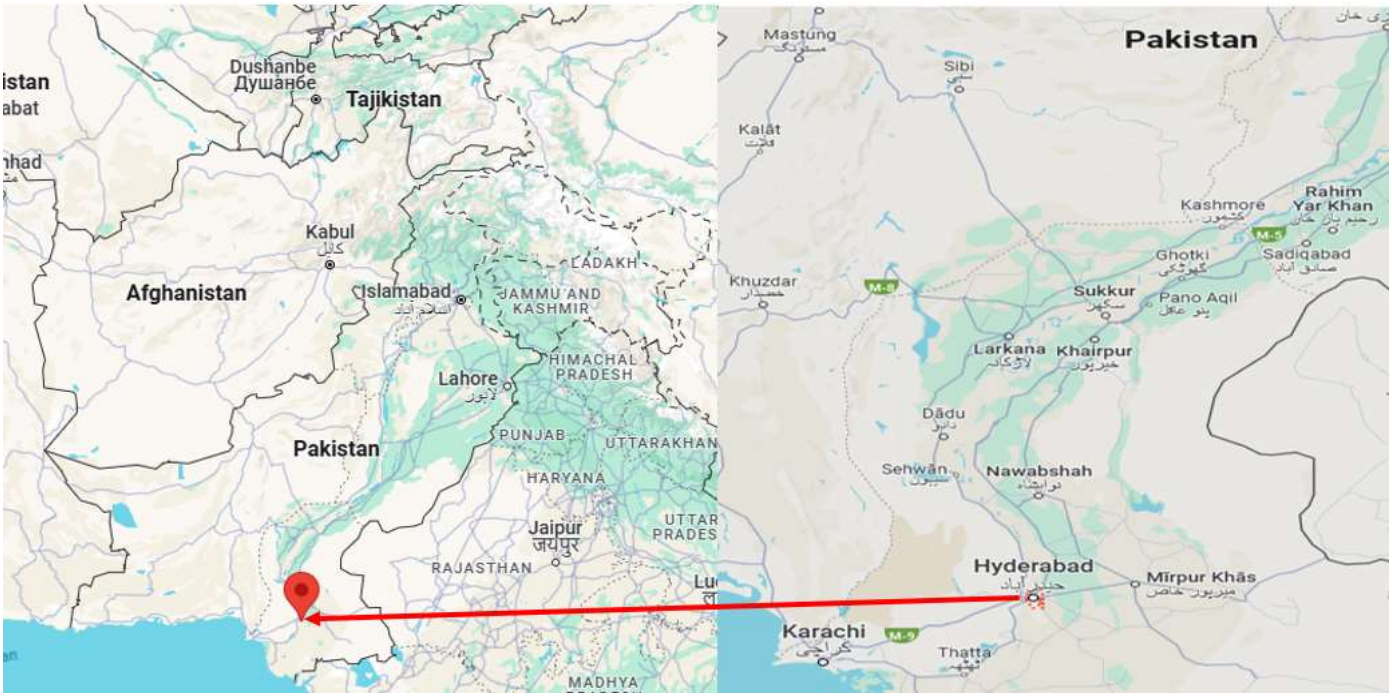

Fig. 1 Geographical location of Sample collection.

behaviour and physical characteristics of the lipstick plasma produced during LIBS analysis by examining plasma parameters such as electron temperature, electron number density, plasma frequency, and inverse bremsstrahlung coefficient.

2. MATERIAL

Lipstick samples of different brands were collected from local market of Hyderabad, Sindh, Pakistan. The details about samples are given in Table 1 and the geographical location of sample collection is given in Fig. 1.

3. EXPERIMENTATION

Experimental setup is defined in our previous work [18]. Fig. 2 shows a schematic of the entire experimental setup. A Q-switched Nd: YAG (Quantal Brilliant) pulsed laser (532 nm), with pulse duration of 5 ns and frequency of 10 Hz, is employed as the energy source to generate plasma. The sample was positioned over an adjustable sample stage that was kept at a distance within the focusing lens's focal length, a 20 cm focal length quartz convex lens, to prevent air disruption. Since the laser pulse causes a crater on the sample's surface during the ablation process, the sample is rotated at different angles to prevent a deep hole and to offer a new surface after each laser pulse. The optical fiber with a collimating lens (0-45° field of view), positioned at right angles to the direction of the plasma expansion, collects the light generated by the plasma plume. The collected light is then registered using the LIBS2000 spectrometer (Ocean Optics. Inc).

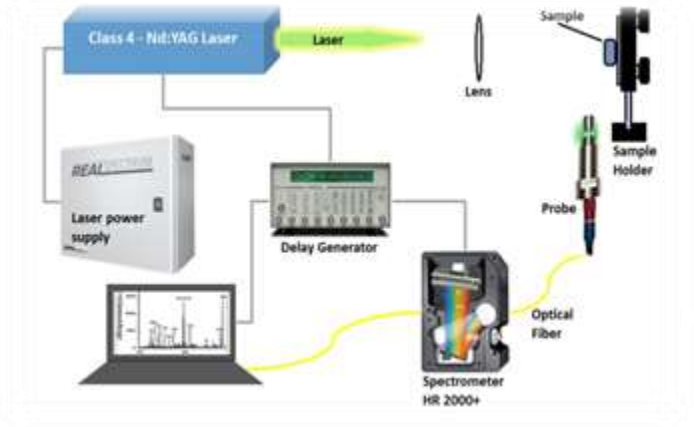

Fig. 2 LIBS experimental setup

4. RESULT AND DISCUSSION

4.1. Emission Spectra of Lipstick Plasma

At the post experimental stage, we have observed Mercury (Hg), Cobalt (Co), Chromium (Cr) Lead (Pb), Iron (Fe), Titanium (Ti), Molybdenum (Mo), Potassium (K), Calcium (Ca) and Sodium (Na) in lipstick plasma. The emission spectrum of lipsticks plasma consisted of spectral lines of Fe-I at (357.01, 358.11, 363.14, 364.78, 373.48, 373.71, 374.55, 374.94, 404.50, 406.35, 407.17, 430.79, 432.57, 440.47, 522.71, 523.29, 526.95 and 532.85) nm, Fe-II at (234.34, 234.83, 238.20, 238.86, 239.56, 239.92, 240.48, 241.05, 258.58, 259.94, 260.70, 261.18, 262.56, 263.13, 273.95,

Table: 1. Detail information about samples

S. No	Lipstick Samples	
	Class	Sample
1	0	Christine Princess
2	1	Genny Frost
3	2	Madame Gabriela
4	3	Medora

274.32, 274.65 and 275.75) nm, C-I at 247.85 nm, K-II 373.13 nm, Ca-I at 649.37 nm, Ca-II at (393.36 and 396.99) nm, Al-I at (394.40 and 396.15) nm, Cr-I at (425.43, 427.48 and 553.54) nm, Pb-I at 401.96 nm, Pb-II at 438.60 nm, Co-I at 412.13 nm, Co-II at 414.51 nm, Mo-I at 444.22 nm, Ba-I at 705.99 nm, Ba-II at (455.40, 493.40 and 614.17) nm, Zn-II at 492.32 nm, Mg-I at 516.73 nm, Cd-II at 537.80 nm, Na-I at (588.99 and 589.59) nm, H-I at 656.28 nm and Li-I at 670.77 nm shown in Fig. 3 (a-f). The transition lines are documented via NIST database [19].

4.2. Spatial Variation of Plasma Emission

In order to study the thermodynamic behaviour of the lipstick plasma we have registered the spectrum at different distances normal to the plasma plume. In the spatial variation of the transition lines we have noticed that the intensity of the emission lines is maximum at 0 mm spatial distance and observed to be decreasing as the distance increases due the thermalization and recombination phenomenon. Spatial variation of Barium ion at 455.40 nm is shown in Fig. 4 (a). The comparison of full spectra at different spatial distance gives a decreasing trend in the intensity of spectral lines Fig. 4 (b).

4.3. Chemometric Analysis

Chemometric tools, specifically Principal Component Analysis (PCA) and Linear Discriminant Analysis (LDA), were employed to distinguish the lipstick samples. PCA, an unsupervised method, is used to reduce the dimensionality of large datasets by maximizing the variance within the data. It transforms a large set of variables into a smaller set while preserving most of the original information. These reduced variables are called principal components (PCs), each carrying a certain portion of the original information. The first principal component holds the largest amount of information, with each subsequent component containing progressively less. In contrast, LDA is a supervised classification technique designed to project features from a higher-dimensional space onto a lower-dimensional space. While PCA focuses on maximizing the variance in the data, LDA aims to maximize the separation between different data groupings. LDA calculates directions, known as linear discriminants, which represent the axes that maximize the separation between classes.

In this study, PCA and LDA were combined to observe the clustering of lipstick samples. PCA was performed on the entire spectral data within the wavelength range of 200 - 720 nm. One key feature of PCA is the scores, which describe the properties of the samples and can be represented as a map where one PC is plotted against another, illustrating the similarities or differences between samples. Each sample has a score on each PC, reflecting its position along that component. For the lipstick samples, Fig. 5 Shows the variance ratios of principal components obtained from Principal Component Analysis (PCA). The x-axis represents the number of principal components, ranging from 1 to 10, while the y-axis shows the cumulative explained variance ratio for the first n principal components. The blue line indicates how the cumulative explained variance ratio increases as more principal components are included. Notably, the graph shows a steep rise initially, with the first two components capturing approximately 60% of the variance. This is followed by a more gradual increase, with the first eight components explaining 95.4% of the total variance, as highlighted by the red dot. Fig. 6 presents a 2-D projection of the dataset using Principal Component Analysis (PCA), visually representing the variance captured by the first two principal components. Each point in the scatter plot signifies an individual data instance, color-coded by class label as indicated in the legend. The x-axis represents the first principal component, accounting for the greatest variance in the dataset, while the y-axis shows the second principal component, orthogonal to the first and capturing the second highest variance. The observed separation and clustering of different colors reveal the inherent class structure within the data. Notably, classes 0 and 3 form distinct clusters with minimal overlap, indicating clear separability in this reduced dimensional space. In contrast, classes 1 and 2 exhibit a higher degree of overlap, suggesting similarities in their feature distributions. This visualization enhances the understanding of the data's underlying structure, highlighting areas of potential class confusion and separability, which are essential for subsequent model development and evaluation.

Fig. 7 shows the diagonal class represent the percentage of correctly classified instances for each class, while the off-diagonal class highlight the misclassifications. Class 1 and 2 are 100% perfectly classified with 0 % misclassification. While for class 0 represents 91% classification and 9% misclassification which match with class 2. Moreover, class 3 shows accuracy rate 91% with 9% matching with class 1.

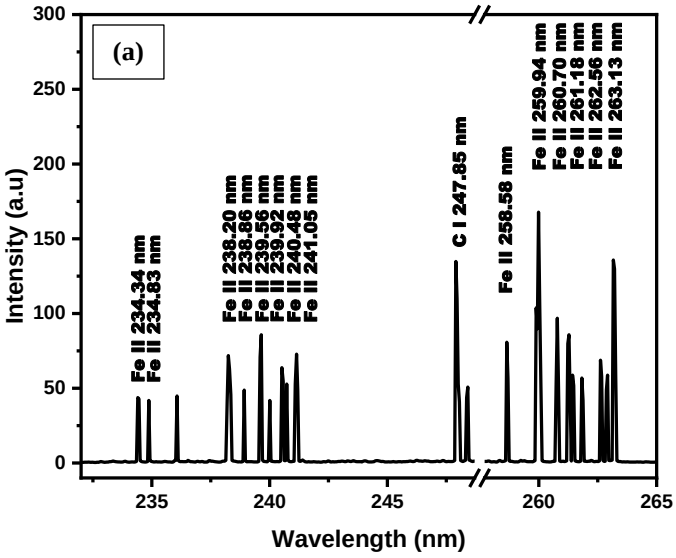
(a)
Fe II 234.34 nm
Fe II 234.83 nm
Fe II 238.20 nm
Fe II 238.86 nm
Fe II 239.56 nm
Fe II 239.92 nm
Fe II 240.48 nm
Fe II 241.05 nm
C I 247.85 nm
Fe II 258.58 nm
Fe II 259.94 nm
Fe II 260.70 nm
Fe II 261.18 nm
Fe II 262.56 nm
Fe II 263.13 nm
Intensity (a.u)
Wavelength (nm)

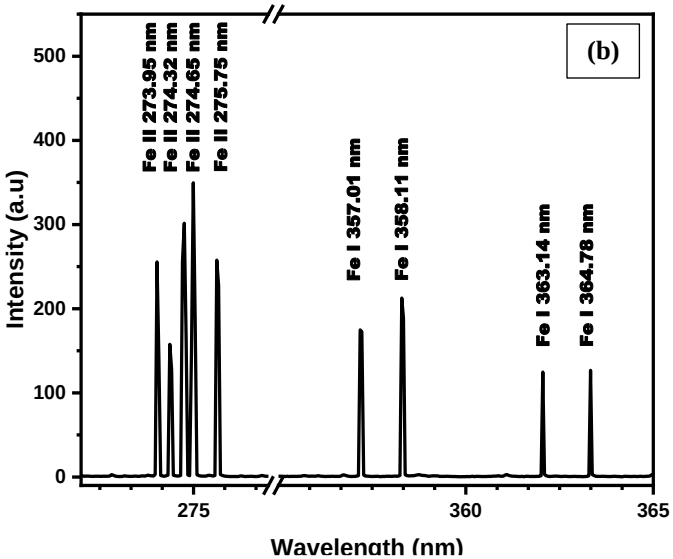
(b)
Fe II 273.95 nm
Fe II 274.32 nm
Fe II 274.65 nm
Fe II 275.75 nm
Fe I 357.01 nm
Fe I 358.11 nm
Fe I 363.14 nm
Fe I 364.78 nm
Intensity (a.u)
Wavelength (nm)

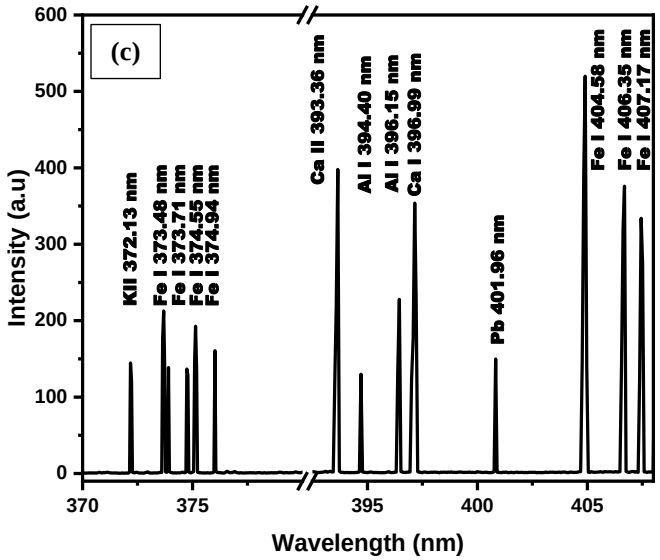
(c)
KII 372.13 nm
Fe I 373.48 nm
Fe I 373.71 nm
Fe I 374.55 nm
Fe I 374.94 nm
Ca II 393.36 nm
Al I 394.40 nm
Al I 396.15 nm
Ca I 396.99 nm
Pb 401.96 nm
Fe I 404.58 nm
Fe I 406.35 nm
Fe I 407.17 nm
Intensity (a.u)
Wavelength (nm)

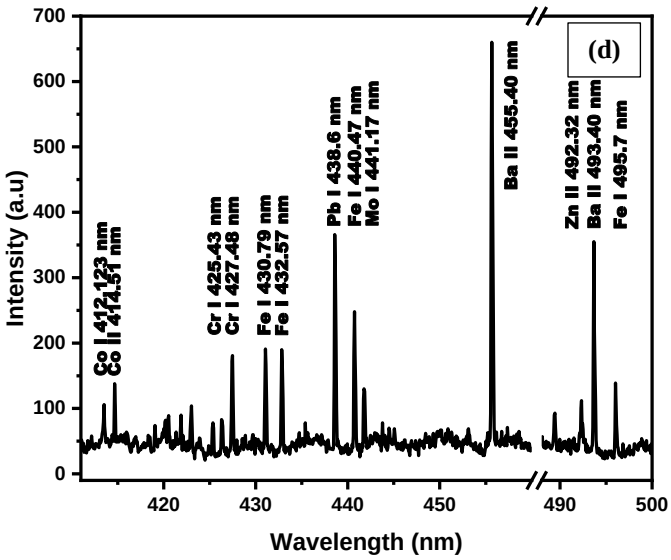
(d)
Co I 412.123 nm
Co II 414.31 nm
Cr I 425.43 nm
Cr I 427.48 nm
Fe I 430.79 nm
Fe I 432.57 nm
Pb I 438.6 nm
Fe I 440.47 nm
Mo I 441.17 nm
Ba II 455.40 nm
Zn II 492.32 nm
Ba II 493.40 nm
Fe I 495.7 nm
Intensity (a.u)
Wavelength (nm)

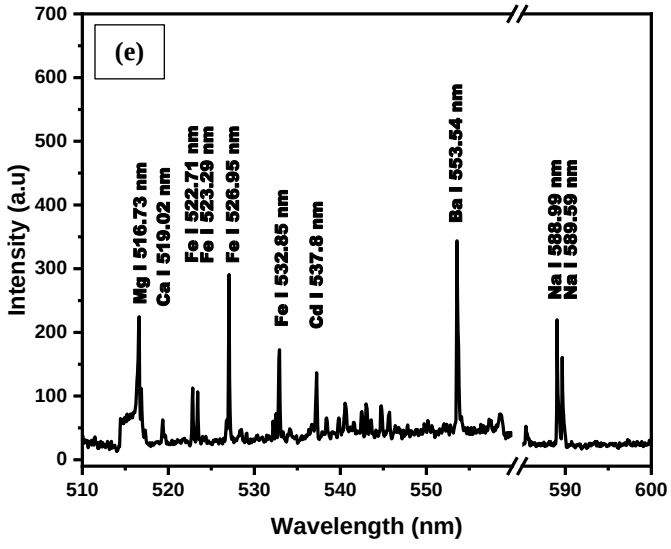
(e)
Mg I 516.73 nm
Ca I 519.02 nm
Fe I 522.71 nm
Fe I 523.29 nm
Fe I 526.95 nm
Fe I 532.85 nm
Cd I 537.8 nm
Ba I 553.54 nm
Na I 588.99 nm
Na I 589.59 nm
Intensity (a.u)
Wavelength (nm)

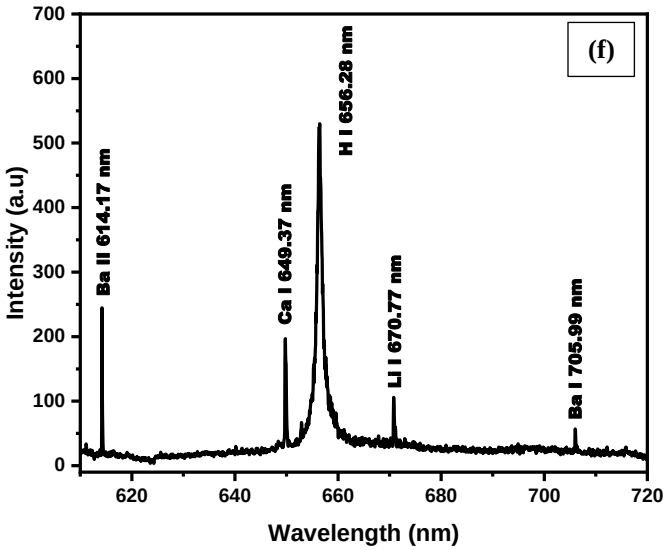
(f)
Ba II 614.17 nm
Ca I 649.37 nm
H I 656.28 nm
LI I 670.77 nm
Ba I 705.99 nm
Intensity (a.u)
Wavelength (nm)

Fig. 3 (a-f) Emission spectra of laser produced lipstick plasma

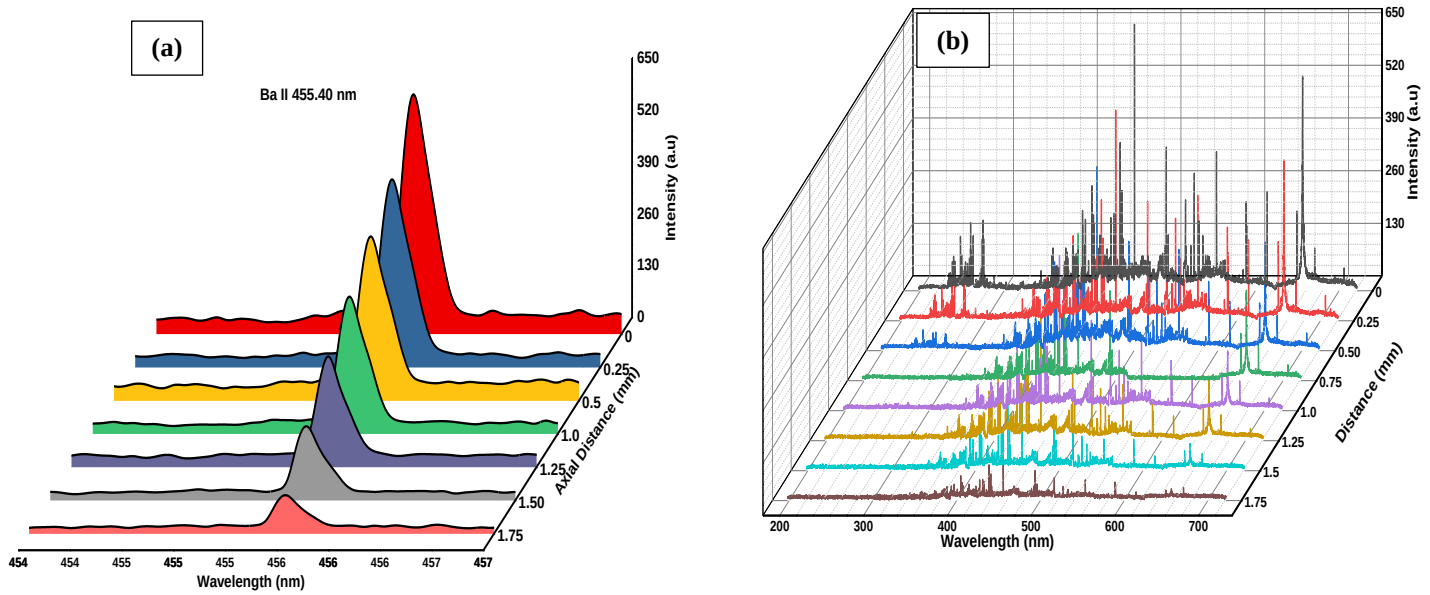

Fig. 4 (a) Spatial variation of Ba–II at 455.40 nm with axial distance (0–1.75) nm. (b) Spatial variation spectral lines with axial distance (0–1.75) nm

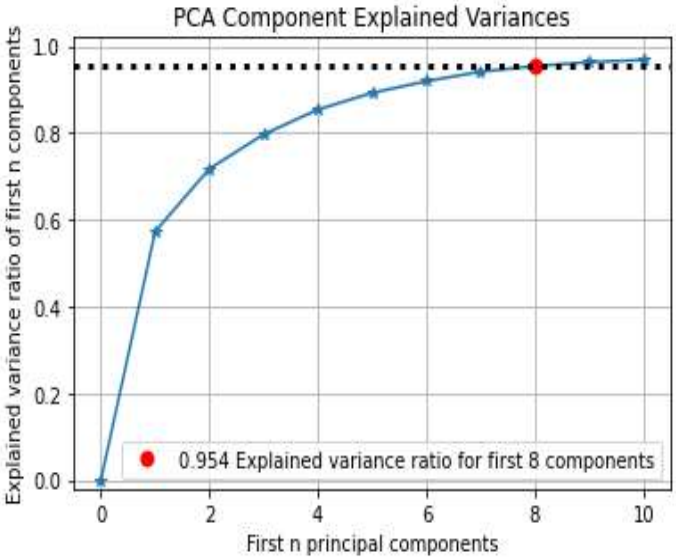

Fig. 5 PCA Component Explained Variances (PCA-EV) for Lipstick data.

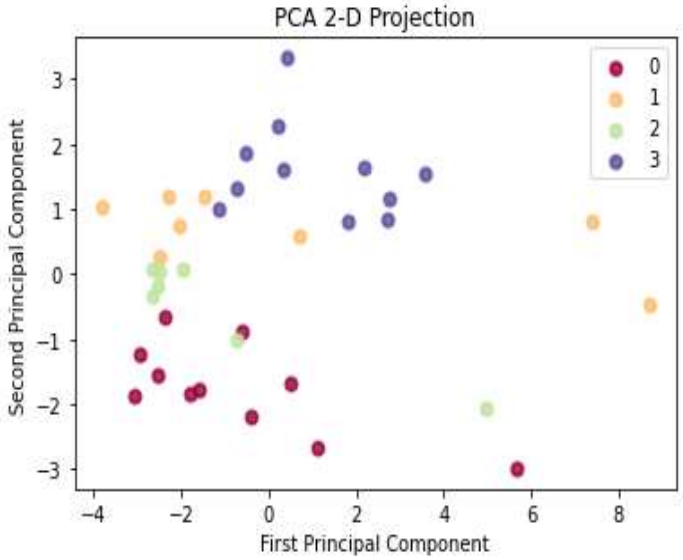

Fig. 6 Scatter plot of PCA for Lipstick data.

4.4. Plasma Parameters

4.4.1 Electron Temperature

When describing plasma states, electron temperature is essential. Eq.1 describes the intensity ratio method we used to determine the plasma temperature.

$$\frac{I_1}{I_2} = \frac{g_1}{g_2}\frac{A_1}{A_2}\frac{\lambda_2}{\lambda_1} e^{\left[-\left(\frac{E_1-E_2}{kT}\right)\right]} \quad (1)$$

With the help of two Fe-I lines, this technique produced a plasma temperature estimate of about 6000 K with a 20% experimental uncertainty. Spatiotemporal temperature change is depicted in Fig. 8, where a reduction is observed with increasing axial distance.

First, absorption of laser radiation via inverse bremsstrahlung is credited with the highest electron temperature since it causes a quick transition from thermal to kinetic energy. Temperatures naturally drop as the plasma expands.

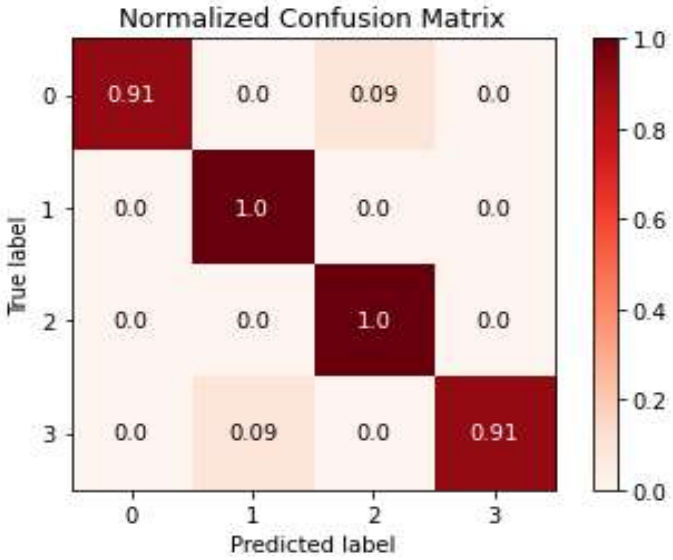

Fig. 7 Normalized Confusion Matrix illustrating the classification performance across four classes, showing high accuracy with minimal misclassifications.

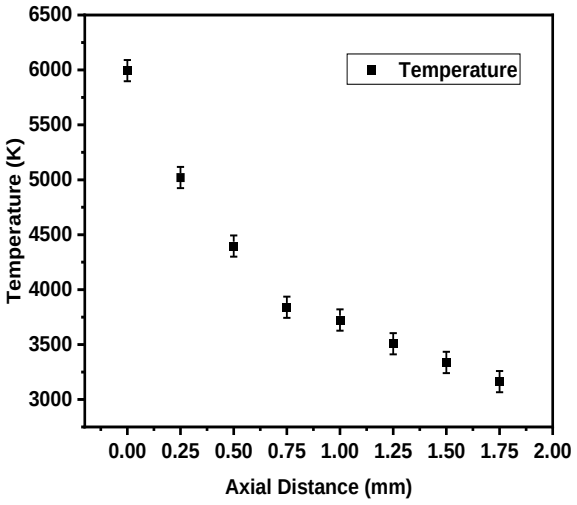

Fig. 8 Variation in the electron temperature with respect to the axial distance.

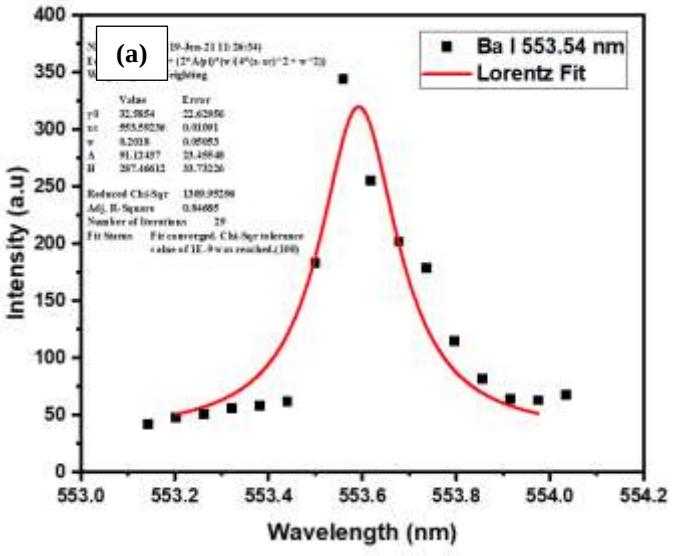

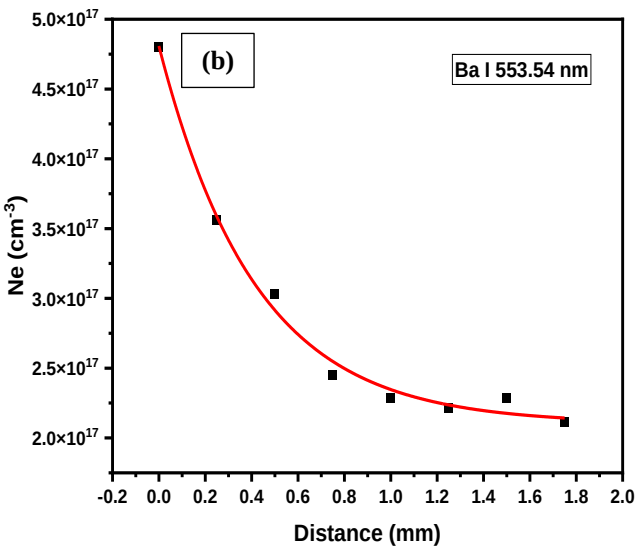

Fig. 9 (a) Stark broadening profile of Ba I 553.54 nm by Lorentz Fit showing FWHM. (b) Spatial behavior electron number density with respect to the distance from 0 to 1.75mm

4.4.2 Electron Number Density

An important factor in determining the thermodynamic equilibrium of lipstick plasma generated by laser is the electron number density. It was ascertained from the Stark broadening profile of a well defined neutral Ba transition line peak at 553.34 nm using Eq. 2. The electron number density was determined to be [20].

$$\lambda_{\frac{1}{2}} = 2\omega\left(\frac{N_e}{10^{16}}\right) \quad (2)$$

Where $\lambda_{\frac{1}{2}}$ is the Stark width, ω is the electron impact parameter and N_e is the electron number density. The electron number density was determined to be $4.80 \times 10^{17}\ cm^{-3}$ at a distance of 0 mm axial from the plasma plume. This number is in excellent agreement with the requirements for local thermodynamic equilibrium (LTE). The electron number density, as shown in Fig. 9 (a-b), peaks nearest to the plasma source and declines progressively from 0 mm to 1.75 mm axial distance. This fluctuation is explained by the sample's and the resultant plasma's continual absorption of laser energy through processes such as photoionization and inverse bremsstrahlung.

4.4.3 Inverse Bremsstrahlung Coefficient

The energy transfer from the plasma to the surrounding gas, which affects the plasma's characteristics and the precision of spectroscopic measurements, is governed by the inverse bremsstrahlung coefficient (IBC) in LIBS. It can be determined using Eq. 3.

$$\alpha_{IB} = 1.37 \times 10^{-35}\ \lambda^3 N_e^2\ T_e^{-1/2} \qquad (3)$$

Where, α_{IB} is inverse-bremsstrahlung coefficient, λ is the wavelength of the laser used, N_e is the electron number density and T_e is the electron temperature [20]. Its sensitivity to longer wavelengths is indicated by the coefficient's dependence on the cubed laser wavelength. The IBC has a peak at 6.15×10^{-3}cm^{-1} at 0 mm axial distance and diminishes as axial distance decreases. Fig.10 shows how the IBC varies in space as a function of distance from the plasma source.

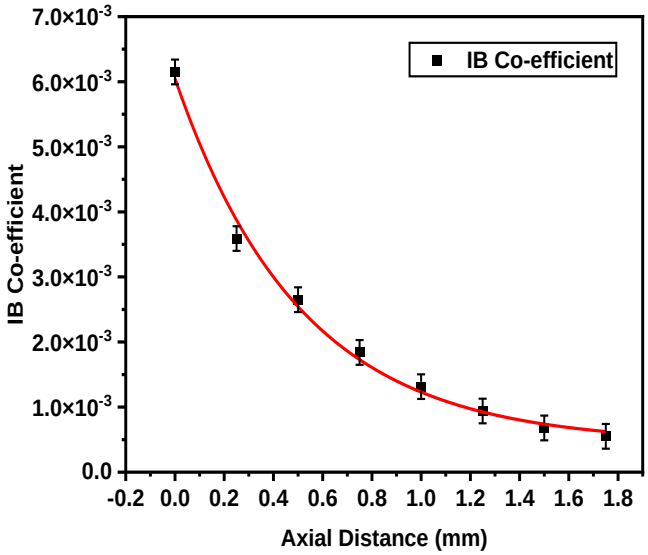

Fig. 10 Spatial variation in the inverse-bremsstrahlung co-efficient with respect to the axial distance.

4.4.4 Plasma Frequency

Plasma frequency is the characteristic frequency at which the charged particles in a plasma oscillate collectively in response to an external perturbation. It is determined by the density and charge of the particles in the plasma. In a plasma, the collective motion of the charged particles can be described by plasma waves. These waves have a characteristic frequency known as the plasma frequency, which is given by:

$$\nu_p = \sqrt{\frac{N_e\, e^2}{\epsilon_o m}} \qquad (4)$$

where N_e is the electron number density, e is the elementary charge, m is the mass of an electron, and ϵ_o is the permittivity of free space [21]. Eq. 4 can further be reduced to [18].

$$\nu_p = 9 \times 10^3 \sqrt{N_e} \qquad (5)$$

Using Eq. 5, it analyzed that plasma frequency is maximum i-e. $6.24 \times 10^{12} Hz$ at 0 mm axial distance and falls exponentially as the distance increases from 0 mm to 1.75 mm as shown in Fig. 11.

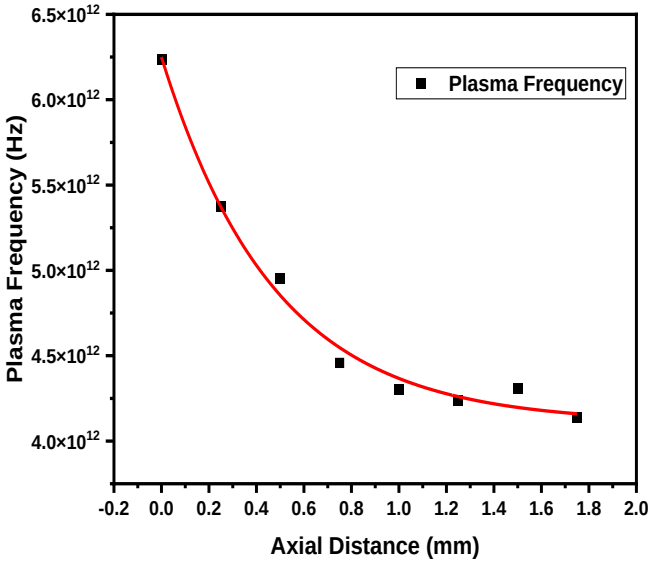

Fig. 11 Variation in the plasma frequency relative to the axial distance from 0 mm to 1.75 mm.

4.5 Calibration Free LIBS (CF-LIBS)

Weight percentage of different analyzed element can be determined by using the different plasma parameter through calibration free LIBS technique. Saha Boltzmann equation is utilized to calculate the weight percentage of both the neutral atoms (C_s^Z) and ions (C_s^{Z+1}) as given in Eq. (7-8) respectively [21].

$$n_e \frac{C_s^{Z+1}}{C_s^Z} = \frac{(2m_e KT)^{\frac{3}{2}}}{h^3} \frac{2U_{Z+1}}{U_Z} \exp\left[-\frac{E_{ion}}{KT}\right] cm^{-3} \qquad (6)$$

$$FC_s^Z = I^{ki} \frac{U_s(T)}{A_{ki}\, g_k}\, e^{\left(\frac{E_k}{kT}\right)} \qquad (7)$$

$$FC_s^{Z+1} = I^{ki} \frac{U_s(T)}{A_{ki}\, g_k}\, e^{\left(\frac{E_k}{kT}\right)} \qquad (8)$$

Where F is the experimental factor associated to the mass ablation (determined through normalizing the species concentration), C_s^z is the neutral species concentration in plasma, I^{ki} is the integrated intensity of transition line, $U_s(T)$ is the partition function, A_{ki} is for transition probability, g_k is the statistical weight, k is Boltzmann constant and T is electron temperature. The total concentration of atomic and ionized particles is presented as [21].

$$C_s^t = C_s^Z + C_s^{Z+1} \quad (9)$$

Weight percentage of different elements found in lipsticks plasma is given in Table 2.

Table 2. Weight percentage of main elements found in the lipstick plasma

Elements	Fe	C	Co	Cr	Pb	Ba	Ba	Si	Al
Wt%	6.32	0.28	86.12	2.33	0.368	0.96	0.96	0.32	0.13

5. CONCLUSION

We found that the Lipstick plasma consisted of Iron (Fe), Carbon (C), Cobalt (Co), Chromium (Cr), Lead (Pb), Molybdenum (Mo), Barium (Ba), Zinc (Zn) Magnesium (Mg), Calcium (Ca), Cadmium (Cd), Potassium (K), Aluminum (Al), Sodium (Na), Hydrogen (H) and Lithium (Li). The existence of Lead, Chromium and Cadmium may cause toxicity. The PCA and LDA were performed based on LIBS data collected from different brands of Lipstick samples. Cobalt is found to be at maximum concentration. It is also found that the plasma temperature and the electron number density were maximum at 0 mm axial distance. The plasma temperature falls from 6000 K to 3162 K as the axial distance is increased from 0 mm to 1.75 mm. Same behaviour of electron number density is also recorded. This variation is due to the thermalization and cooling process in plasma. Plasma frequency and inverse bremsstrahlung co-efficient were also found to be maximum at 0 mm axial distance and recorded to be falling from $6.24 \times 10^{12} Hz$ and $6.15 \times 10^{-3} \text{cm}^{-1}$ respectively as the axial distance is increased from 0 mm to 1.75 mm.

REFERENCES

[1] E. L. Sainio, R. Jolanki, E. Hakala, and L. Kanerva, "Metals and arsenic in eye shadows," Contact dermatitis, vol. 42, no. 1, pp. 5-10, 2000.

[2] I. Al-Saleh, M. Nester, E. Devol, N. Shinwari, and S. Al-Shahria, "Determinants of blood lead levels in Saudi Arabian schoolgirls," International journal of occupational and environmental health, vol. 5, no. 2, pp. 107-114, 1999.

[3] W. Al-Dahhan, H. Hashim, E. Yousif, and A. F. Alkaim, "Lipsticks Elemental Analysis by Energy Dispersive X-Ray Used as Criminal Evidence," Indian Journal of Forensic Medicine & Toxicology, vol. 14, no. 3, 2020.

[4] P. Gardner, M. Bertino, R. Weimer, and E. Hazelrigg, "Analysis of lipsticks using Raman spectroscopy," Forensic science international, vol. 232, no. 1-3, pp. 67-72, 2013.

[5] B. Joshi, K. Verma, and J. Singh, "A comparison of red pigments in different lipsticks using thin layer chromatography (TLC)," J Anal Bioanal Techniques, vol. 4, no. 157, p. 2, 2013.

[6] T. TABTIMSRI and O. Kheawpum, "Analysis of Lipstick Samples by X-ray Diffraction (XRD) Technique for Forensic Applications," Silpakorn University, 2023.

[7] P. Pořízka et al., "Multivariate classification of echellograms: a new perspective in Laser-Induced Breakdown Spectroscopy analysis," Scientific Reports, vol. 7, no. 1, p. 3160, 2017.

[8] Q. Zeng et al., "Laser-induced breakdown spectroscopy using laser pulses delivered by optical fibers for analyzing Mn and Ti elements in pig iron," Journal of Analytical Atomic Spectrometry, vol. 30, no. 2, pp. 403-409, 2015.

[9] Y. Tang et al., "Industrial polymers classification using laser-induced breakdown spectroscopy combined with self-organizing maps and K-means algorithm," Optik, vol. 165, pp. 179-185, 2018.

[10] X. Yang et al., "Simultaneous determination of La, Ce, Pr, and Nd elements in aqueous solution using surface-enhanced laser-induced breakdown spectroscopy," Talanta, vol. 163, pp. 127-131, 2017.

[11] M. E. Sigman, Application of laser-induced breakdown spectroscopy to forensic science: analysis of paint and glass samples. National Center for Forensic Science and Department of Chemistry, University …, 2010.

[12] T. Hussain and M. Gondal, "Laser induced breakdown spectroscopy (LIBS) as a rapid tool for material analysis," in Journal of Physics: Conference Series, 2013, vol. 439, no. 1: IOP Publishing, p. 012050.

[13] I. A. AI-Saleh and L. Coate, "Lead exposure in Saudi Arabia from the use of traditional cosmetics and medical remedies," Environmental Geochemistry and Health, vol. 17, pp. 29-31, 1995.

[14] M. Gondal, Z. Seddigi, M. Nasr, and B. Gondal, "Spectroscopic detection of health hazardous contaminants in lipstick using laser induced breakdown spectroscopy," Journal of hazardous materials, vol. 175, no. 1-3, pp. 726-732, 2010.

[15] S. Liu, S. K. Hammond, and A. Rojas-Cheatham, "Concentrations and potential health risks of metals in lip products," Environmental Health Perspectives, vol. 121, no. 6, pp. 705-710, 2013.

[16] M. Asmaa and S. A. Habana, "Measurement of Plasma Parameters of Fe-Lines in Lipstick Using Laser-Induced Breakdown Spectroscopy," NeuroQuantology, vol. 19, no. 10, p. 1, 2021.

[17] M. Abrar, T. Iqbal, M. Fahad, M. Andleeb, Z. Farooq, and S. Afsheen, "Determination of hazardous ingredients in personal care products using laser-induced breakdown spectroscopy," Laser Physics, vol. 28, no. 5, p. 056002, 2018.

[18] S. Jamali et al., "Elemental analysis of Kohl using laser ablation and atomic absorption spectroscopy (AAS) techniques," Physica B: Condensed Matter, vol. 620, p. 413278, 2021.

[19] J. E. Sansonetti and W. C. Martin, "Handbook of basic atomic spectroscopic data," Journal of physical and chemical reference data, vol. 34, no. 4, pp. 1559-2259, 2005.

[20] S. Jamali et al., "Spectroscopic analysis of lithium fluoride (LiF) using laser ablation," IJCSNS, vol. 19, no. 8, pp. 127-134, 2019.

[21] S. Jamali et al., "Elemental analysis of talcum powder using spectroscopic techniques," Optik, vol. 261, p. 169246, 2022.